

Viscous Extension of the Unsteady Vortex Lattice Method

Pol Mesalles Ripoll* University of California, Irvine, CA, 92697

Amir Saman Rezaei[†] University of California, Irvine, CA, 92697

Haithem Taha‡ University of California, Irvine, CA, 92697

In this study, the standard unsteady vortex lattice method (UVLM) is modified by different approaches to accommodate the viscous effects on the flow field and lift force history of a moving airfoil. Firstly, the conventional inviscid vortices are replaced with ones that satisfy Oseen's approximation of the Navier-Stokes equations. These are known as viscous vortices and are a function of the Reynolds number. Compared to the standard UVLM, the results show a different behavior for the wake deformation at lower Reynolds numbers where the viscous effects are more dominant. The second modification is implemented by an elegant alteration in the conservation of circulation condition based on the fact that the whole domain composed of the fluid and solid can be treated as a single kinematic entity. The no-slip boundary condition enables considering the moving solid vorticity in the Kelvin condition, where the results for the frequency response indicate more phase lag compared to the standard UVLM or potential flow theories (i.e., Theodorsen), which increases at higher reduced frequencies. Furthermore, the effect of the position of the shed vortices is analyzed and seen to affect the amplitude of the resulting lift history. Finally, the no-slip boundary condition is also explicitly considered by implementing source singularities along the surface of a thick airfoil, resulting in a better prediction of the lift magnitude compared to CFD results. The combination of all the aforementioned modifications has the potential to enhance the performance of the UVLM in case of viscous flows at relatively high reduced frequencies.

I. Nomenclature

angle of attack α C_l lift coefficient C_p pressure coefficient

chord length

distribution of circulation γ

Γ total circulation Γ_{B} bound circulation Γ_W wake circulation = k reduced frequency ν kinematic viscosity freestream pressure p_{∞} velocity potential field

 Re_c chord-based Reynolds number

fluid density

 U_{∞} freestream velocity

^{*}Junior Specialist, Department of Mechanical and Aerospace Engineering.

[†]PhD Student, Department of Mechanical and Aerospace Engineering, AIAA Member.

[‡]Assistant Professor, Department of Mechanical and Aerospace Engineering, AIAA Member.

II. Introduction

Unsteady aerodynamics are present in major engineering applications, including wing flutter, flapping, and complex maneuvers often performed by military aircraft that involve a sudden change in their configuration. These unconventional phenomena also occur at low Reynolds numbers in the flight of insects and bio-inspired micro air vehicles [1]. To study these effects, the unsteady vortex lattice method (UVLM) aims to provide more accurate solutions than analytical efforts —such as Theodorsen, Wagner, and Von Kármán and Sears— by allowing the wake to deform, while taking considerably less computational time than any Navier—Stokes CFD solver [2] or even more efficient schemes for temporal periodic problems [3].

Our goal is to extend the standard 2D UVLM code to better predict the time history of the lift of a moving airfoil—which is the main metric that concerns us— by considering the effects of viscosity. Enhanced analytical approaches in potential flow and several modifications to the original UVLM exist [4–7], though most of them deal with unsteady point vortices or the leading-edge vortex effects that occur at high angles of attack [8] and high Reynolds numbers, but do not account for the viscous effects on low deflection movements of the airfoil. To address this, viscosity has been implemented in vorticity-based methods [9, 10], but the approach presented here is different as it makes use of the analytical results obtained from the Oseen's approximation of Navier–Stokes equations.

The Kutta condition and the conservation of circulation are the two most controversial conditions [2, 11] in the potential flow framework that can be modified to enhance the performance of the potential-based methods. In the standard UVLM methodology, only the no-penetration boundary condition is taken into account when programming the solver. In the present technique, the conservation of circulation is altered both directly and indirectly to also satisfy the no-slip boundary condition on the surface of the traveling body, resulting in a more realistic approach.

By incorporating the changes that will be introduced below into the standard UVLM, the method has the potential to capture the weak nonlinearities of the lift history that are present, for instance, at moderate Reynolds numbers right before the transition is expected [12]. For this study, though, we will focus on airfoils at low Reynolds numbers and low angles of attack to evaluate the significance of each correction in a standard case.

III. Methodology

A. The original UVLM

The standard UVLM code that is considered as the foundation of this work is presented by Katz and Plotkin [13]. Such a method is the unsteady extension of the discrete vortex method, which uses lumped-vortex elements over the camberline to represent a lifting thin airfoil. The equations that follow summarize this method when using a frame of reference that moves with the freestream, a more common approach in aerodynamic simulations than the one presented in [13].

Since this is a potential analysis where the flow is assumed to be irrotational, the velocity field can be written as the gradient of a scalar:

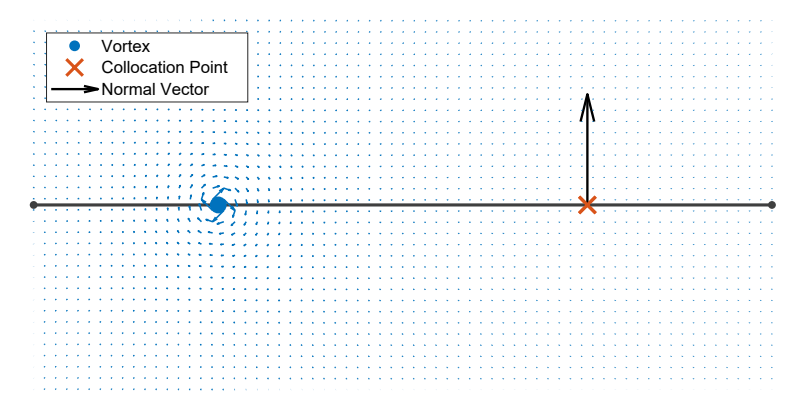
$$\boldsymbol{u} = \nabla \phi \tag{1}$$

and considering the fluid to be incompressible, the main equation describing the velocity potential is derived:

$$\nabla^2 \phi = 0 \tag{2}$$

The chosen lumped-vortex singularity (point vortex) already satisfies Eq. (2), and since the problem is linear and admits superposition, a distribution of these elements along the airfoil also follows the governing equation. Thus, the problem can be solved subject to a given boundary condition. It can be seen that the Kutta condition mentioned in the Introduction is not a necessary constraint that needs to be implemented for this method to function, though it will be implicitly considered by the panel discretization described below.

The numerical approach for solving this case consists in dividing the airfoil camber line in N panels and then - indicated and a second common to the second commo computing t1discretization es are evaluated at the three-



Vortex collocation point and normal vector for a single panel

In this case, as the airfoil acts like a streamline, the no-penetration boundary condition is used as follows:

$$(\mathbf{u}_{\infty} + \nabla \phi_B) \cdot \mathbf{n} = 0 \tag{3}$$

where $u_{\infty} = U_{\infty}(\cos \alpha, \sin \alpha)$, $\nabla \phi_B$ is the perturbation (induced velocity) caused by the bound vortices over the camber line, and n is the normal vector to each panel.

The induced velocity at a point (x_i, y_i) due to a singular vortex placed at coordinates (x_i, y_i) follows the Biot–Savart law:

$$\boldsymbol{u}_{ij} = \frac{\Gamma}{2\pi r^2} \begin{bmatrix} 0 & 1\\ -1 & 0 \end{bmatrix} \begin{bmatrix} x_i - x_j\\ y_i - y_j \end{bmatrix}$$
(4)

where Γ is the circulation generated by the vortex and $r^2 = (x_i - x_j)^2 + (y_i - y_j)^2$.

For the i-th panel then, Eq. (3) becomes:

$$\boldsymbol{u}_{\infty} \cdot \boldsymbol{n}_{i} + \sum_{i=1}^{N} \boldsymbol{u}_{ij} \cdot \boldsymbol{n}_{i} = 0 \tag{5}$$

From the previous equation, a matrix form can easily be constructed for the whole airfoil:

$$\begin{bmatrix} a_{11} & a_{12} & \cdots & a_{1N} \\ a_{21} & a_{22} & \cdots & a_{2N} \\ \vdots & \vdots & \ddots & \vdots \\ a_{N1} & a_{N2} & \cdots & a_{NN} \end{bmatrix} \begin{bmatrix} \Gamma_1 \\ \Gamma_2 \\ \vdots \\ \Gamma_N \end{bmatrix} = \begin{bmatrix} RHS_1 \\ RHS_2 \\ \vdots \\ RHS_N \end{bmatrix}$$
(6)

where $a_{ij} = u_{ij} \cdot n_i$ are called the influence coefficients (computed for $\Gamma_i = 1$), and RHS_i = $-u_{\infty} \cdot n_i$. $\Gamma_1, \Gamma_2, \dots, \Gamma_N$ represent the circulation distribution over the airfoil, and can be used to obtain the loads, the pressure distribution, and the resulting lift coefficient.

When transitioning to the unsteady model, the whole steady code is placed inside a time loop, and in each iteration the airfoil position is updated following a prescribed motion. In order to take into account the unsteady effects, the wake must be considered. In this case, the wake is represented by N_W discrete vortices convecting with the freestream and the induced velocities. To do that, a new vortex Γ_{WN_W} is shed from the trailing edge (or near the trailing edge) at each time-step t_k . To find its value, Kelvin's circulation conservation theorem is used:

$$\frac{\mathrm{D}\Gamma}{\mathrm{D}t} = 0\tag{7}$$

and hence:

$$\sum_{i=1}^{N} \Gamma_i(t_k) + \sum_{i=1}^{N_W} \Gamma_{Wi} = 0$$
 (8)

or equivalently:

$$\sum_{i=1}^{N} \Gamma_{i}(t_{k}) + \Gamma_{WN_{W}} = -\sum_{i=1}^{N_{W}-1} \Gamma_{Wi} = \sum_{i=1}^{N} \Gamma_{i}(t_{k-1}) \equiv \Gamma_{B}(t_{k-1})$$
(9)

Hence, Eq. (6) is modified to account for the shed vortices in the wake and the following system of equations is obtained:

$$\begin{bmatrix} a_{11} & a_{12} & \cdots & a_{1N} & a_{1W} \\ a_{21} & a_{22} & \cdots & a_{2N} & a_{2W} \\ \vdots & \vdots & \ddots & \vdots & \vdots \\ a_{N1} & a_{N2} & \cdots & a_{NN} & a_{NW} \\ 1 & 1 & \cdots & 1 & 1 \end{bmatrix} \begin{bmatrix} \Gamma_{1}(t_{k}) \\ \Gamma_{2}(t_{k}) \\ \Gamma_{2}(t_{k}) \\ \vdots \\ \Gamma_{N}(t_{k}) \\ \Gamma_{WN_{W}} \end{bmatrix} = \begin{bmatrix} RHS_{1} \\ RHS_{2} \\ \vdots \\ RHS_{N} \\ \Gamma_{B}(t_{k-1}) \end{bmatrix}$$
(10)

where a_{iW} 's are the influence coefficients at the collocation points of the newly shed vortex. It is worth noting that these coefficients are only computed once as they only depend on the airfoil shape and not on its position.

On the unsteady case, besides seeing the freestream velocity, the airfoil can also be moving following a certain maneuver, so the right-hand side coefficients from Eq. (10) must be corrected as follows:

$$RHS_i = -(u_{\infty} - u_i) \cdot n_i \tag{11}$$

where u_i is the velocity of the collocation point i due to the airfoil motion on an inertial frame of reference.

As it has been said, the wake vortices are convected downstream. To do so, in each iteration the position of a wake vortex i is updated in the following way:

$$\mathbf{r}_{\mathbf{W}i}(t_k) = \mathbf{r}_{\mathbf{W}i}(t_{k-1}) + \mathbf{u}_{\mathbf{W}i}\Delta t \tag{12}$$

where Δt is the time increment at each time-step and u_{wi} is computed taking into account the freestream and the induced velocities by the bound and the other wake vortices:

$$u_{Wi} = u_{\infty} + \sum_{j=1}^{N} u_{ij} + \sum_{j=1, j \neq i}^{N_W} u_{ij}$$
(13)

Once the circulation distribution over the airfoil and along the wake is known, the loads can be computed using the unsteady Bernoulli equation:

$$p = -\rho \left(\frac{1}{2} \| \boldsymbol{u} \|^2 + \frac{\partial \phi}{\partial t} \right) \tag{14}$$

Since the goal is to find the pressure difference between the upper and lower surfaces of the camberline:

$$\Delta C_p = C_{pl} - C_{pu} = \frac{2}{U_{\infty}^2} \left\{ \frac{1}{2} \left(u_{u\tau}^2 - u_{l\tau}^2 \right) + \frac{\partial \phi_u}{\partial t} - \frac{\partial \phi_l}{\partial t} \right\}$$
 (15)

where $u_{u\tau}$ and $u_{l\tau}$ are the tangential components of the velocity around the thin airfoil. For a panel i, with tangential vector τ_i and length Δl_i , the velocity is:

$$u_{i\tau} = (\boldsymbol{u}_{\infty} - \boldsymbol{u}_{i} + \boldsymbol{u}_{Wi}) \cdot \boldsymbol{\tau}_{i} \pm \frac{\partial \phi}{\partial \tau_{i}} \approx (\boldsymbol{u}_{\infty} - \boldsymbol{u}_{i} + \boldsymbol{u}_{Wi}) \cdot \boldsymbol{\tau}_{i} \pm \frac{1}{2} \frac{\Gamma_{i}}{\Delta l_{i}}$$
(16)

and the time derivative, making use of the relation $\phi = \int_{LE}^{x} \frac{\partial \phi}{\partial x} dx = \int_{LE}^{x} \frac{\gamma}{2} dx$, becomes:

$$\frac{\partial \phi_i}{\partial t} \approx \frac{\partial}{\partial t} \sum_{j=1}^{i} \frac{\Gamma_j}{2} \tag{17}$$

Finally, Eq. (15) for the thin airfoil case can be written as follows:

$$\Delta C_{pi} \approx \frac{2}{U_{\infty}^{2}} \left\{ (\boldsymbol{u}_{\infty} - \boldsymbol{u}_{i} + \boldsymbol{u}_{Wi}) \cdot \boldsymbol{\tau}_{i} \frac{\Gamma_{i}}{\Delta l_{i}} + \frac{\partial}{\partial t} \sum_{j=1}^{i} \Gamma_{j} \right\}$$
(18)

where the time derivative is numerically approximated using a first order scheme. Then, a vector force coefficient can be calculated:

$$\Delta C_{Fi} = (\Delta C_{pi} \Delta l_i) \, n_i \tag{19}$$

and finally, the lift coefficient is obtained:

$$C_{l} = \frac{1}{c} \sum_{i=1}^{N} \Delta C_{Fi} \cdot (-\sin \alpha, \cos \alpha)$$
 (20)

where α is the constant angle of attack between the x-axis and the freestream, not to be confused with the instantaneous variation of angle of attack $\alpha(t)$ of the moving airfoil.

B. Viscous extension of the UVLM

The proposed viscous extension of the UVLM is derived from the analytical work by Shen and Crimi [14] on an oscillating thin airfoil, which at the same time is based on the Oseen's approximation. The latter takes the well-known Navier–Stokes continuity and momentum equations for incompressible flow:

$$\nabla \cdot \boldsymbol{u} = 0$$

$$\frac{\partial \boldsymbol{u}}{\partial t} + (\boldsymbol{u} \cdot \nabla) \, \boldsymbol{u} = -\frac{1}{\rho} \nabla p + \nu \nabla^2 \boldsymbol{u} + \boldsymbol{g}$$
(21)

and linearizes them in the 2D case about the solution $u_{\infty} = u_{\infty}\hat{i}$ and p_{∞} . Hence, $u = u_{\infty} + u'$, $p = p_{\infty} + p'$, and the expanded form of Eq. (21), neglecting the body forces and second-order terms, results:

$$\frac{\partial u'}{\partial x} + \frac{\partial v'}{\partial y} = 0$$

$$\frac{\partial u'}{\partial t} + u_{\infty} \frac{\partial u'}{\partial x} = -\frac{1}{\rho} \frac{\partial p'}{\partial x} + \nu \nabla^{2} \mathbf{u'}$$

$$\frac{\partial v'}{\partial t} + u_{\infty} \frac{\partial v'}{\partial x} = -\frac{1}{\rho} \frac{\partial p'}{\partial y} + \nu \nabla^{2} \mathbf{u'}$$
(22)

Defining the linear differential operator $\mathcal{A} \equiv \left[\frac{\partial}{\partial t} + u_{\infty} \frac{\partial}{\partial x} - \nu \nabla^2 \right]$, Eq. (22) can be further simplified:

$$\nabla \cdot \boldsymbol{u}' = 0$$

$$\mathcal{A}\boldsymbol{u}' = -\frac{1}{\rho} \nabla p'$$
(23)

Given the linearity of the Oseen's approximation, if the solution of the velocity field is considered as the sum of an irrotational and a rotational term:

$$u' = \nabla \phi + u_r \tag{24}$$

then it follows that the pressure distribution is independent from the rotational contribution:

$$p = -\rho \mathcal{A}\phi = -\rho \left(\frac{\partial \phi}{\partial x} + u_{\infty} \frac{\partial \phi}{\partial t} \right)$$
 (25)

Eq. (25) is the linearized form of the same unsteady Bernoulli equation from Eq. (14), which can be used to compute the loads. On the other hand, the rotational term of the velocity must satisfy:

$$\nabla \cdot \boldsymbol{u_r} = 0$$

$$\mathcal{A}\boldsymbol{u_r} = 0$$
(26)

Shen and Crimi modeled a flat plate with bound vortices and sources, and found the velocity distribution due to these singularities that fulfills the Oseen's approximation. From their solution, a viscous expression for the velocity u_B induced by a viscous bound vortex to replace Eq. (4) is derived:

$$\boldsymbol{u_{Bij}} = \frac{\Gamma}{2\pi} \left\{ \left(\frac{1}{r} - \sigma e^{\sigma(x_i - x_j)} K_1(\sigma r) \right) \frac{1}{r} \begin{bmatrix} 0 & 1 \\ -1 & 0 \end{bmatrix} \begin{bmatrix} x_i - x_j \\ y_i - y_j \end{bmatrix} - \sigma e^{\sigma(x_i - x_j)} K_0(\sigma r) \begin{bmatrix} 0 \\ 1 \end{bmatrix} \right\}$$
(27)

where K_0 and K_1 are modified Bessel functions of the second kind, while $\sigma = \frac{\text{Re}_c}{4}$. Unlike the inviscid function, Eq. (27) depends on both r and x. This behavior is reminiscent from Yates' viscous kernel [15], which is basically the 1D version of Shen and Crimi's expression:

$$K(x) = \frac{1}{x} + \sigma e^{\sigma x} \left(K_0 \left(\sigma |x| \right) - K_1 \left(\sigma |x| \right) \operatorname{sgn} x \right)$$
 (28)

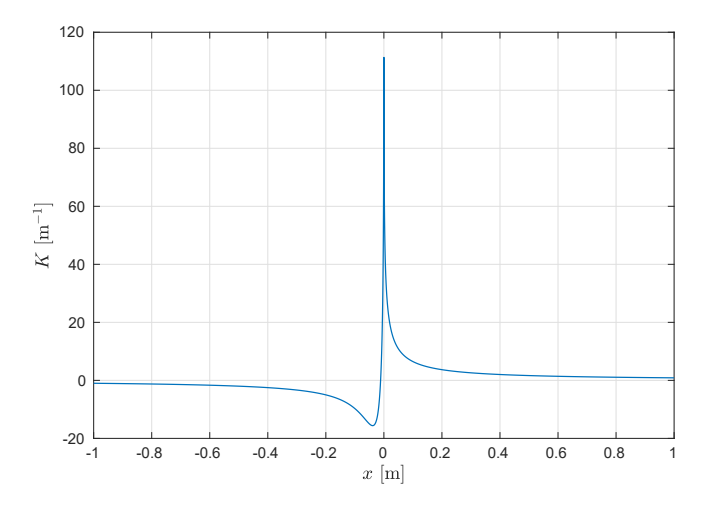


Figure 2 Yates' viscous kernel at a very low Reynolds number (Re = 100) to show the difference between the downstream and the upstream (positive and negative values of x, respectively)

When plotting Eq. (28) in Fig. 2, it can be seen that it is not symmetric as there is a slight difference between positive and negative values of x, which represent the downstream and the upstream of the vortex respectively [16]. However, this dissimilarity is negligible at higher Reynolds numbers, and given that the numerical implementation of the original Eq. (27) (based on Yates' kernel) causes issues when dealing later with the thickness implementation, only the downstream side will be considered.

The previous assumption has leads to the following simplification for the induced velocity, which has been checked to provide the same results for thin airfoils:

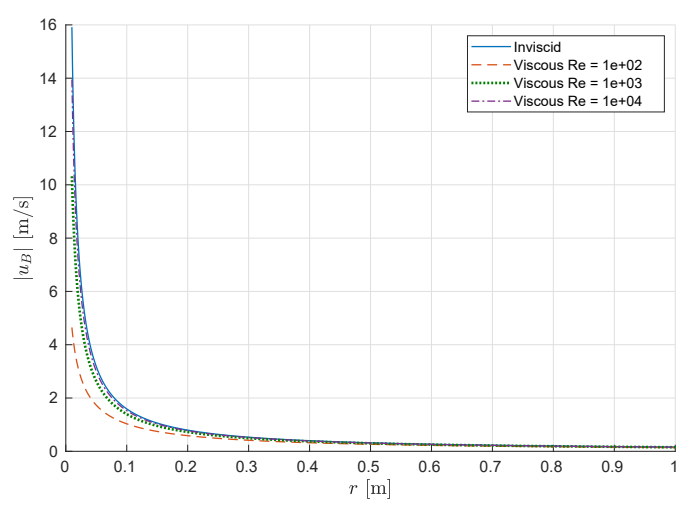
$$\boldsymbol{u_{Bij}} \approx \frac{\Gamma}{2\pi r} \left\{ \frac{1}{r} + \sigma e^{\sigma r} \left(K_0 \left(\sigma r \right) - K_1 \left(\sigma r \right) \right) \right\} \begin{bmatrix} 0 & 1 \\ -1 & 0 \end{bmatrix} \begin{bmatrix} x_i - x_j \\ y_i - y_j \end{bmatrix}$$
(29)

Fig. 3a shows how this new function compares to the original inviscid Biot-Savart at different Reynolds numbers.

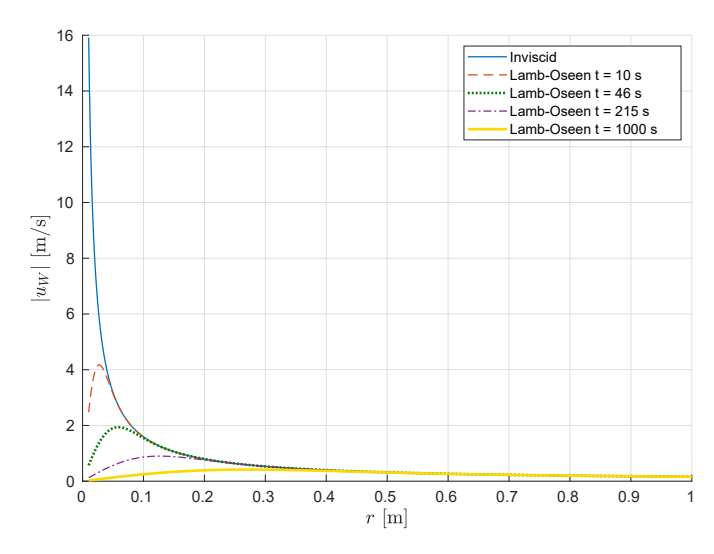
On the other hand, Shen and Crimi considered the wake as a sheet of vortices of decaying strength over time. Thus, their induced velocity u_W can be represented by the Lamb–Oseen function:

$$\boldsymbol{u_{Wij}} = \frac{\Gamma}{2\pi r^2} \left\{ 1 - \exp\left(-\frac{r^2}{4\nu \left(t_k - t_s\right)}\right) \right\} \begin{bmatrix} 0 & 1\\ -1 & 0 \end{bmatrix} \begin{bmatrix} x_i - x_j\\ y_i - y_j \end{bmatrix}$$
(30)

where t_s is the time when a particular wake vortex was first shed. Fig. 3b shows how this new function compares to the original inviscid Biot–Savart at different times t_k .



(a) Inviscid and viscous bound vortex functions at different Reynolds numbers

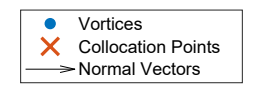


(b) Inviscid and viscous wake vortex functions at different times after shedding with $v = 1.48 \times 10^{-5} \text{ m}^2/\text{s}$

Figure 3 Bound and wake vortices satisfying Oseen's approximation compared to the inviscid counterpart

C. Thickness implementation

With very few modifications, the existing UVLM code is capable of working with thick airfoils, which is relevant when dealing with viscous flows. Panels are placed along the upper and lower surfaces instead of the camberline, while keeping the exact same geometry discretization regarding the position of vortices at the quarter chord and collocation points at the three-quarter chord, resulting in a setup like the one in Fig. 4.



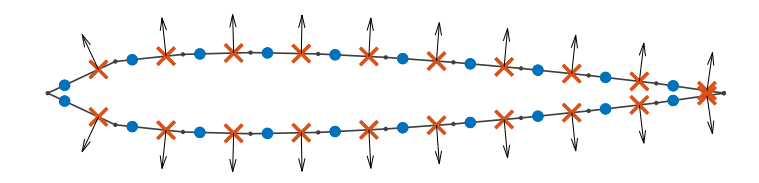


Figure 4 Geometry discretization for a thick NACA 0012 airfoil with N=20 panels, showing the vortices at the quarter chord, the collocation points at the three-quarter chord, and the normal vectors

The main difference in this case is related to the calculation of the lift coefficient. Instead of working with the pressure difference, the thickness implementation uses the total pressure coefficient. From Eq. (14), it follows:

$$C_p = 1 - \left(\frac{\|\boldsymbol{u}\|}{U_{\infty}}\right)^2 - \frac{2}{U_{\infty}^2} \frac{\partial \phi}{\partial t} \tag{31}$$

For a panel i over a stagnant moving airfoil, the following relation holds true:

$$\gamma_i = \|\mathbf{u}\| - \mathbf{u}_i \cdot \mathbf{\tau}_i \tag{32}$$

and thus the pressure coefficient on each panel can be obtained. Then, one can find the vector force coefficient:

$$C_{Fi} = (C_{pi}\Delta l_i)(-n_i) \tag{33}$$

which is used to compute the final lift coefficient:

$$C_{l} = \frac{1}{c} \sum_{i=1}^{N} C_{Fi} \cdot (-\sin\alpha, \cos\alpha)$$
(34)

D. Adding sources

To fully implement the Shen and Crimi viscous extension, bound sources are added over the airfoil beside the vortices, enabling us to also satisfy the no-slip boundary condition. In order to do that, the system from Eq. (10) is expanded to include N new equations:

$$\begin{vmatrix} a_{\gamma 11} & a_{\gamma 12} & \cdots & a_{\gamma 1N} & a_{q11} & a_{q12} & \cdots & a_{q1N} & a_{\gamma 1W} & a_{q1W} \\ a_{\gamma 21} & a_{\gamma 22} & \cdots & a_{\gamma 2N} & a_{q21} & a_{q22} & \cdots & a_{q2N} & a_{\gamma 2W} & a_{q2W} \\ \vdots & \vdots & \ddots & \vdots & \vdots & \ddots & \vdots & \vdots & \vdots \\ a_{\gamma N1} & a_{\gamma N2} & \cdots & a_{\gamma NN} & a_{qN1} & a_{qN2} & \cdots & a_{qNN} & a_{\gamma NW} & a_{qNW} \\ b_{\gamma 11} & b_{\gamma 12} & \cdots & b_{\gamma 1N} & b_{q11} & b_{q12} & \cdots & b_{q1N} & b_{\gamma 1W} & b_{q1W} \\ b_{\gamma 21} & b_{\gamma 22} & \cdots & b_{\gamma 2N} & b_{q21} & b_{q22} & \cdots & b_{q2N} & b_{\gamma 2W} & b_{q2W} \\ b_{\gamma N1} & b_{\gamma N2} & \cdots & b_{\gamma NN} & b_{qN1} & b_{qN2} & \cdots & b_{qNN} & b_{\gamma NW} & b_{qNW} \\ \vdots & \vdots & \ddots & \vdots & \vdots & \vdots & \ddots & \vdots & \vdots \\ 1 & 1 & \cdots & 1 & 0 & 0 & \cdots & 0 & 1 & 0 \\ 0 & 0 & \cdots & 0 & 1 & 1 & \cdots & 1 & 0 & 1 & 0 \\ 0 & 0 & \cdots & 0 & 1 & 1 & \cdots & 0 & 1 & 0 \\ 0 & 0 & \cdots & 0 & 1 & 1 & \cdots & 0 & 1 & 0 \\ 0 & 0 & \cdots & 0 & 1 & 1 & \cdots & 0 & 0 & 0 \\ 0 & 0 & \cdots & 0 & 1 & 1 & \cdots & 0 & 0 & 0 \\ 0 & 0 & \cdots & 0 & 1 & 1 & \cdots & 0 & 0 \\ 0 & 0 & \cdots & 0 & 1 & 1 & \cdots & 0 & 0 \\ 0$$

where $a_{\gamma ij}$ are the same influence coefficients from before, and a_{qij} represent the influence of the sources, both for the no-penetration equations. On the other hand, $b_{\gamma ij}$ and b_{qij} are the new influence coefficients due to the no-slip equations, for vortices and sources respectively. They are computed as follows:

$$a_{\gamma ij} = \mathbf{u}_{ij} \cdot \mathbf{n}_{i} \qquad a_{qij} = \mathbf{u}_{Sij} \cdot \mathbf{n}_{i} b_{\gamma ij} = \mathbf{u}_{ij} \cdot \mathbf{\tau}_{i} \qquad b_{qij} = \mathbf{u}_{Sij} \cdot \mathbf{\tau}_{i}$$

$$(36)$$

The velocity u_{ij} induced by the vortices is the same as before, and for the sources the following expression is used:

$$\boldsymbol{u_{Sij}} = \frac{Q}{2\pi r^2} \begin{bmatrix} 1 & 0\\ 0 & 1 \end{bmatrix} \begin{bmatrix} x_i - x_j\\ y_i - y_j \end{bmatrix}$$
(37)

The last two rows from Eq. (35) represent, in the first place, the Kelvin condition for the conservation of circulation from the original method, and secondly, the following condition:

$$\sum_{i=1}^{N} Q_i = 0 \tag{38}$$

which has been found to be a necessary constraint to obtain a physical behavior for the flow wake. Eq. (38) is extracted from [13], where it is stated that for a closed body like an airfoil the net flow generated inside must be zero.

IV. Results

For the results presented in this work, a pitching movement described by a changing instantaneous angle of attack is considered:

$$\alpha(t) = \alpha_0 + A\sin(\omega t) \tag{39}$$

where ω is the angular frequency of the moving airfoil. In our case, this will be the frequency of either the pitching or plunging motion. For most simulations, we will consider a small amplitude of $A = 3^{\circ}$.

In order to evaluate the differences between the viscous UVLM and the inviscid code, besides making use of lift history plot, the following transfer function—equivalent to Theodoresen's function—is presented:

$$F = \frac{C_{lC}}{C_{lQS}} \tag{40}$$

where C_{lC} is the circulatory component of the resulting lift from UVLM, obtained by subtracting from C_l the non-circulatory Theodorsen value C_{lNC} for the studied case. C_{lQS} is directly the quasi-steady lift from Theodorsen. By taking a sinusoidal pitching as the input motion of the airfoil at different values of k from 0.1 to 1.0 and using the Fourier transform, a frequency response analysis can be performed to see the magnitude |F| and the phase shift $\angle F$. For the detailed procedure of finding the frequency response from the lift history, refer to [1].

A. Thin-airfoil viscous UVLM

Below we present the viscous results for a symmetric NACA 0012 airfoil —a flat plate when represented by the camberline—performing pitching at a reduced frequency k=1 hinged at the quarter chord point at two different amplitudes A with $\alpha_0=0$. The numerical parameters are as follows: (i) the freestream velocity is set to $U_{\infty}=1$ m/s, (ii) the number of panels is N=40 over a chord of c=1 m, and (iii) we take a time increment of $\Delta t=0.02$ s and run the analysis for 2 cycles.

In Fig. 5, the resulting lift coefficient is plotted against nondimensionalized time (by the period T) for both the inviscid (original UVLM) and the viscous case at a low Reynolds number of Re = 1000, where the viscous effects are more dominant. For both cases, the results are very close to the analytical Theodorsen solution, except for the overprediction of the magnitude of the total lift coefficient.

Finally, Fig. 6 shows the shape of the wake in the last time-step of the simulation, right before the airfoil starts its third cycle. This graph is obtained by plotting the positions of the wake vortices for the case with pitching amplitude $A = 8^{\circ}$, where it is easier to spot the differences. The results show that as the viscosity becomes more dominant at lower Reynolds numbers, it is increasingly difficult for eddies to start forming downstream. Both the original UVLM and the viscous code at $Re = 10^{5}$ show that the vortices can move more freely, while at $Re = 10^{3}$ their movement is severly limited by the viscosity. The reason behind this change is the decaying strength of the wake vortices from Eq. (30). As time passes, the velocity induced by the viscous vortices decreases, especially at short distances, and thus they have a lesser influence on their immediate surroundings. The bound vortices have been found to have no noticeable effects on the wake shape.

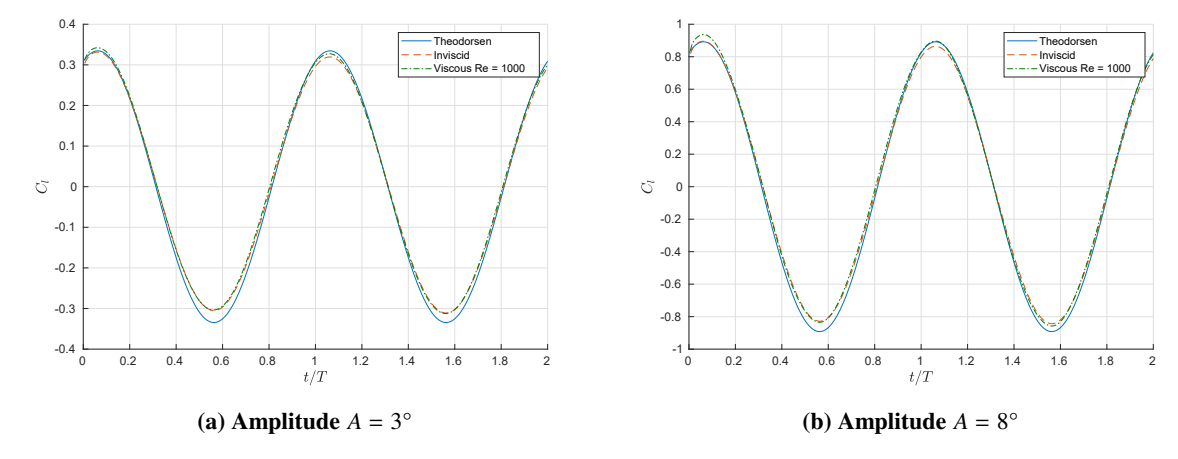
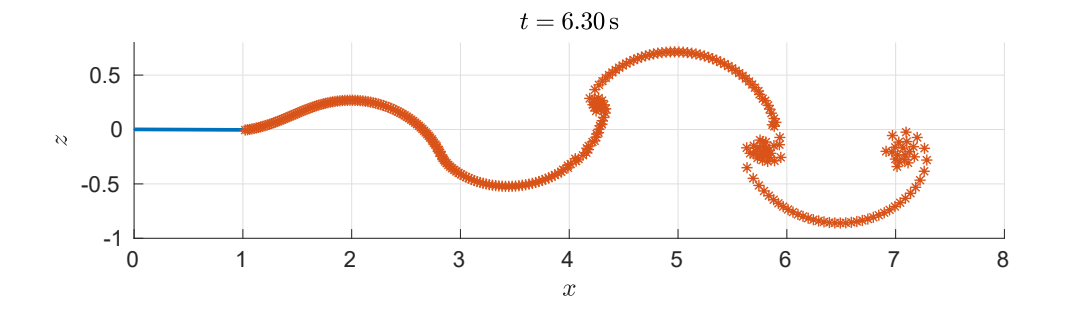
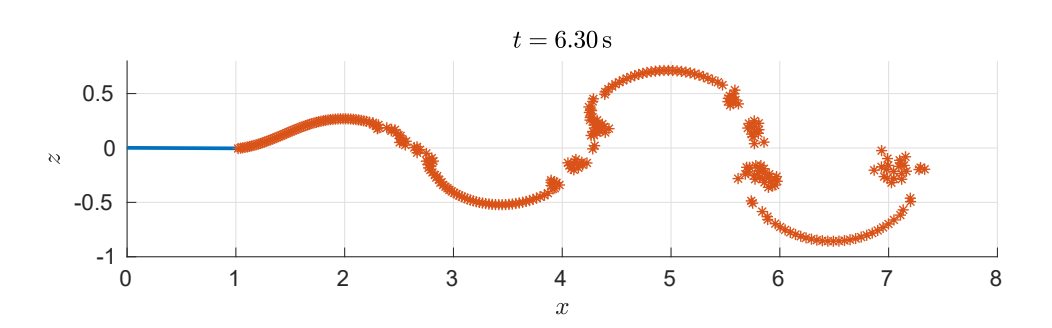


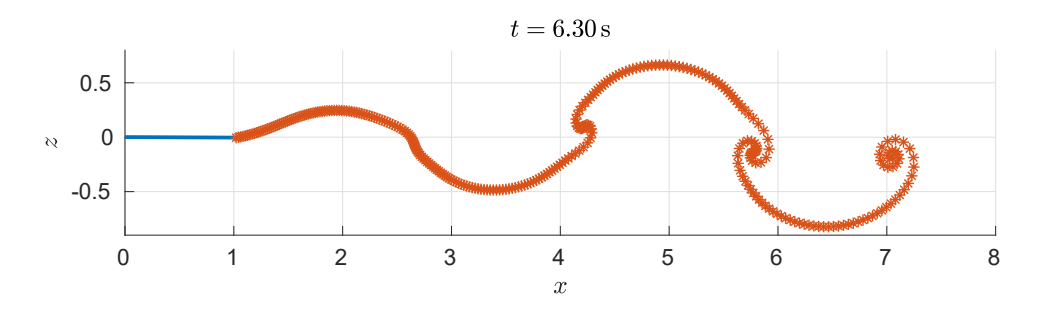
Figure 5 Time history of the lift coefficient at k = 1



(a) Inviscid



(b) Viscous $Re = 10^5$



(c) Viscous $Re = 10^3$

Figure 6 UVLM wake shape deformation

B. On the conservation of circulation

In the case of a moving airfoil, Eq. (7) must be examined carefully. Following Wu [11], the whole fluid-body domain can be considered as a single kinematic system. For the elucidation, consider a revolving spoon inside a cup of tea. Through the no-slip condition between the fluid and solid, the vorticity of the solid is transferred to the fluid medium. In our flapping airfoil case, although the motion of the solid is symmetric (i.e., sinusoidal) and the net effect seems to be zero, the time derivative term in the equations implies hysteresis and the induced forces by the vortices indicate non-zero mean effect. Eq. (41) shows the modified condition to be utilized in the UVLM code:

$$\frac{D\Gamma}{Dt} = \frac{D\Gamma_{\text{fluid}}}{Dt} + \frac{D\Gamma_{\text{solid}}}{Dt} = 0 \tag{41}$$

where Γ_{solid} is the circulation of the solid body. The vorticity of a rotating airfoil of surface area A_{foil} is 2Ω , where Ω is the angular frequency. The circulation is simply the line integral over the body contour, and hence $\Gamma_{solid} = 2\Omega A_{foil}$.

For our numerical approach, Eq. (41) becomes:

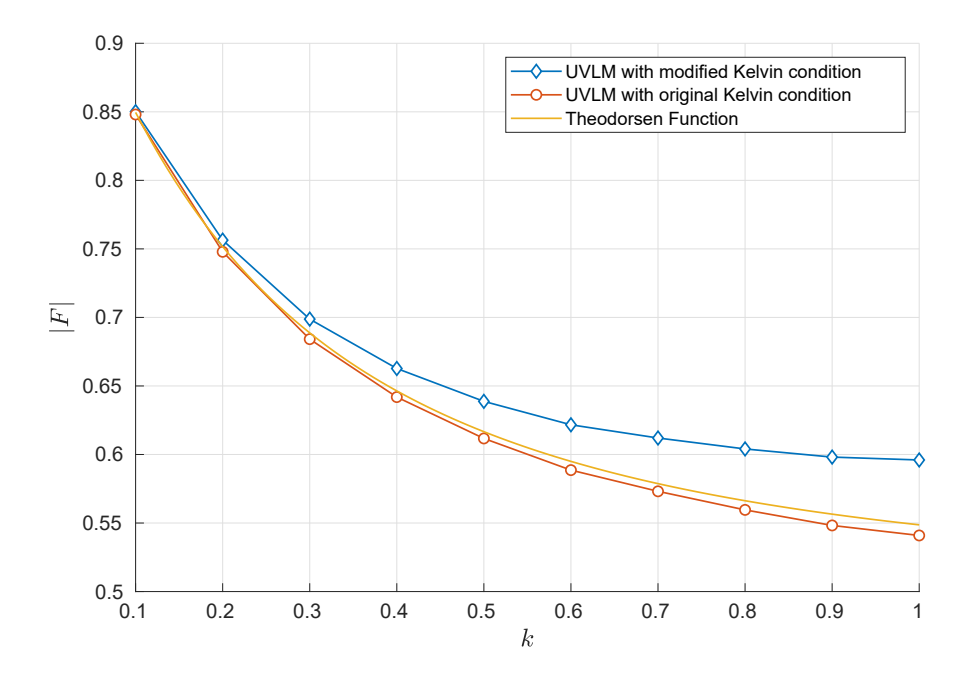
$$\frac{\Gamma_B\left(t_k\right) - \Gamma_B\left(t_{k-1}\right)}{\Delta t} + \frac{\Gamma_W\left(t_k\right) - \Gamma_W\left(t_{k-1}\right)}{\Delta t} + \frac{\Gamma_S\left(t_k\right) - \Gamma_S\left(t_{k-1}\right)}{\Delta t} = 0 \tag{42}$$

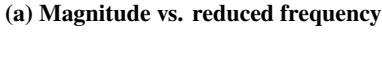
where Γ_B is the total circulation over the airfoil due to bound vortices, Γ_W is the total circulation over the wake, and Γ_S is the circulation of the airfoil solid body. Then, it follows:

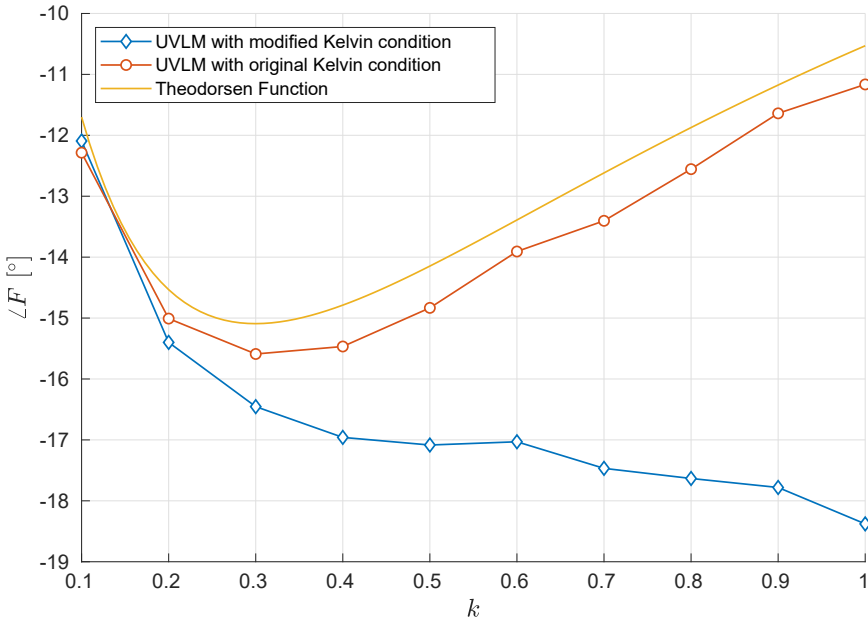
$$\Gamma_B(t_k) + \Gamma_{WN_W} = \Gamma_B(t_{k-1}) - \left[\Gamma_S(t_k) - \Gamma_S(t_{k-1})\right] \tag{43}$$

which can be used to modify the last right-hand side term of Eq. (10) to take into account the solid vorticity.

To assess the significance of the solid body circulation term, a pitching maneuver has been analyzed both neglecting and taking into account this value. The results show a significant change in the phase of the lift time history, and hence a frequency response analysis of the circulatory component of the lift coefficient has been conducted. The results of the latter are presented in Fig. 7, and show a promising behavior that is more similar to the one obtained in CFD simulations where the phase lag increases with the reduced frequency [2].







(b) Phase vs. reduced frequency

Figure 7 Frequency response analysis of the circulatory component of the UVLM with and without the solid body circulation term, along with Theodorsen's solution

C. On the position of the shed vortex

While it may seem intuitive to place the latest shed vortex at the trailing edge, given that we are discretizing what would be an infinite sheet of vortices along the wake with lumped elements, it is suggested that this might not be the most accurate position [13]. The latest wake vortex will always be placed at some point in the trajectory followed by the trailing edge (TE) between one time-step and the next, but instead of positioning it at the TE itself, it can be located at some distance *z* along that path (see Fig. 8).

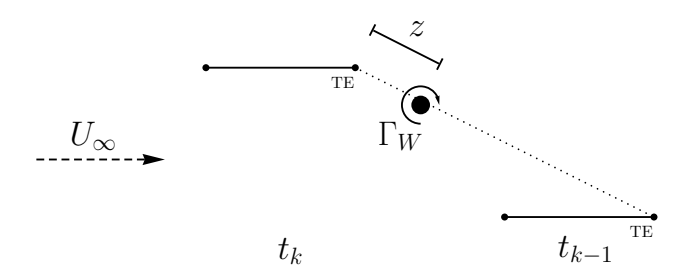


Figure 8 Schematic for the position of the trailing edge vortex Γ_W

Therefore, a pitching maneuver with $A = 3^{\circ}$ and k = 1 has been analyzed to see the importance of this position. Fig. 9 shows the resulting lift coefficient as a function of nondimensional time for different values of z. It can be seen that this number has a direct impact on the amplitude of C_l , and hence the position z = 0—that is, a vortex attached to the trailing edge itself— is selected as the best candidate to take the amplitude closer to CFD results [2].

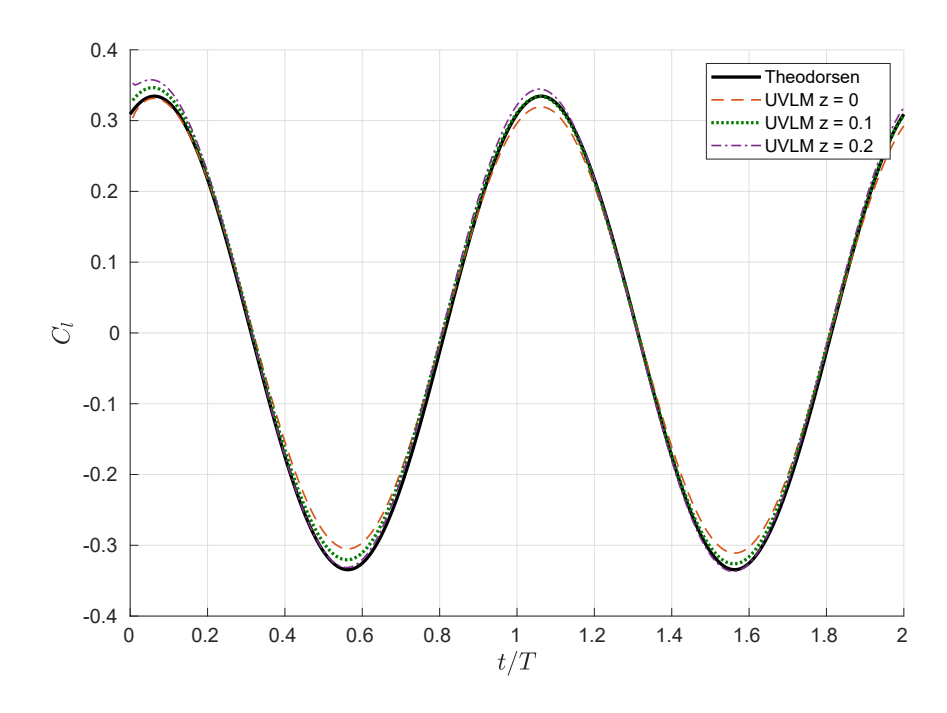


Figure 9 Time history of the lift coefficient for a pitching airfoil changing the position of the shed vortex, where z is expressed as a fraction of the total possible distance with 0 being the closest to the TE

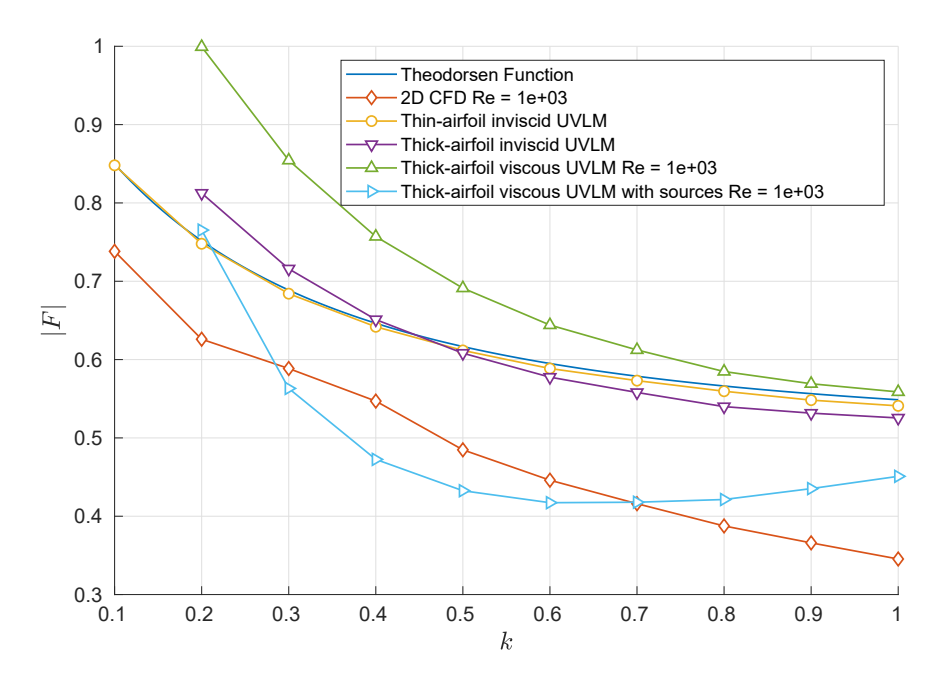
D. Thick-airfoil viscous UVLM

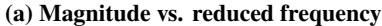
The final version of the modified unsteady vortex lattice method presented in this work is designed for thick airfoils, and each of the following changes have been tested independently: (i) the viscous effects due to both the bound and the wake vortices, (ii) the modified Kelvin condition to implicitly satisfy the no-slip boundary condition, and (iii) the addition of sources to explicitly satisfy the no-slip boundary condition when solving the system of equations. The combination of sources and viscosity has also been analyzed, but in that case the altered conservation of circulation has not been used as that would result in the no-slip condition being considered twice.

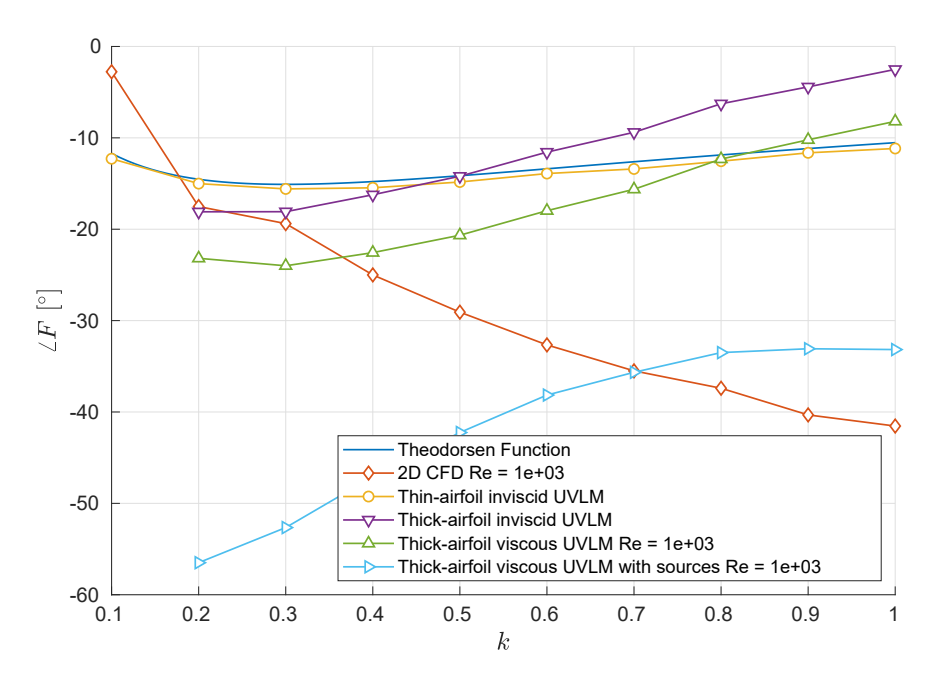
After a convergence study, it has been found that running the code with N=100 elements (50 on each surface) over a chord of c=1 m at $U_{\infty}=1$ m/s and a time-step increment of $\Delta t=0.01$ s strikes the best balance between performance and numerical error in the resulting lift coefficient.

In Fig. 10, the viscous effects can be studied from a set of different frequency response analysis. The plot displays the results of the original thin-airfoil inviscid UVLM along with the thick-airfoil versions of the inviscid UVLM, the viscous UVLM, and the viscous UVLM with added sources. It also includes the analytical Theodorsen function and the results obtained using a 2D CFD laminar solver in ANSYS Fluent. All the simulations are for a pitching motion of amplitude $A = 3^{\circ}$, and the ones that take the viscosity into account have been run at a low Reynolds number of Re = 1000 to represent more clearly its effects. Unlike the thin-airfoil case, when dealing with thickness, the viscous vortices that satisfy Oseen's approximation are seen to have a noticeable effect on both the magnitude and the phase of the lift history (and hence, the transfer function). The magnitude of F is significantly higher at lower reduced frequencies than expected and its phase presents an offset with respect to the inviscid code, leading to increased phase lag for all frequencies. The addition of sources does balance the increased amplitude of the thick-airfoil lift, decreasing the magnitude of F to values that are closer to the ones from high-fidelity CFD simulations. At lower reduced frequencies we see higher phase lag than expected, but starting at k = 0.6 the values are considerably closer to the ANSYS results than any other case.

Finally, Fig. 11 analyzes the effects of each implementation of the no-slip boundary condition. The plot combines results from the inviscid UVLM with the modified Kelvin condition —both with and without thickness— to represent the implicit no-slip condition. It also includes the thick-airfoil UVLM with sources to represents the explicit enforcement of the same boundary condition. To complete the figure, the Theodorsen function is shown, along with the high-fidelity results from 2D CFD simulations at two different Reynolds numbers: $Re = 10^3$ and $Re = 10^5$. The modified conservation of circulation is seen to give better results for the thin-airfoil UVLM than its thick counterpart, especially in terms of phase, even though it still improved the results when compared to the thick-airfoil inviscid UVLM from Fig. 10. Like before, the explicit no-slip boundary condition from the UVLM with added sources results in a frequency response for the magnitude of the transfer function that is more similar to CFD results, but its phase presents more lag at reduced frequencies lower than k = 0.6.

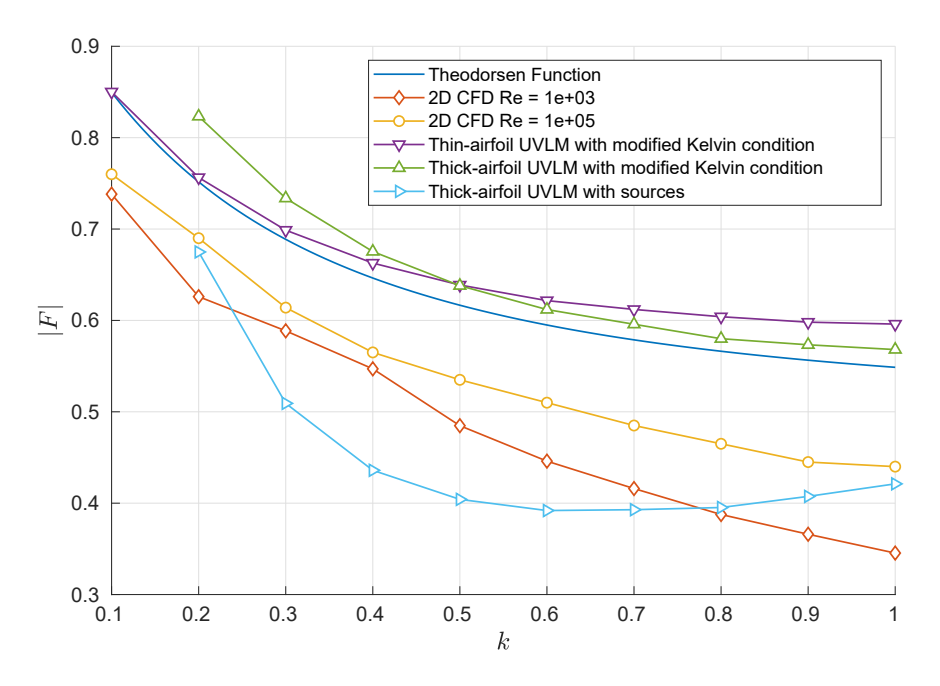


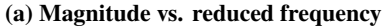


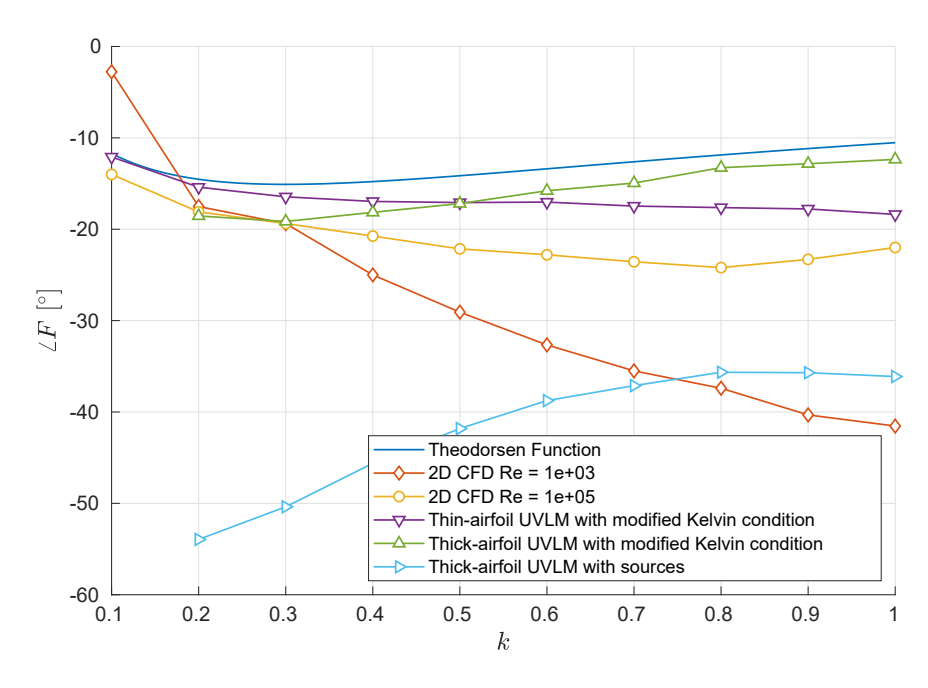


(b) Phase vs. reduced frequency

Figure 10 Frequency response analysis of the circulatory component of the UVLM with thickness, viscosity, and sources







(b) Phase vs. reduced frequency

 $Figure \ 11 \quad Frequency \ response \ analysis \ of \ the \ circulatory \ component \ of \ the \ UVLM \ with \ thickness, \ the \ modified \ Kelvin \ condition, \ and \ sources$

V. Conclusion

In conclusion, some of the modifications of the unsteady vortex lattice method presented in this work can improve the results from the original UVLM, especially for highly viscous flows at relatively high reduced frequencies, where the new code is capable of providing more accurate lift dynamics in considerably less amount of time.

Viscosity has been considered by replacing the original inviscid vortices with ones that satisfy the Oseen's approximation. These changes are found to have a negligible effect on the lift history when using the thin-airfoil approach of UVLM, but they increase the phase lag when thickness is considered. The wake shape does presents a different behavior at lower Reynolds, where the wake vortices stop large eddies from forming downstream.

Altering the Kelvin condition by considering the fluid-body domain as a single entity enables us to to implicitly satisfy the no-slip boundary condition on the surface of the moving airfoil. This modification of the conservation of circulation indicates more phase lag at higher reduced frequencies in comparison to the standard model.

Finally, the addition of sources over a thick airfoil results in a significant reduction of the lift magnitude, bringing its value close to CFD simulations. At high reduced frequencies, the phase lag is also comparable with the one from such solvers.

References

- [1] Rezaei, A. S., and Taha, H. E., "Computational Study of Lift Frequency Responses of Pitching Airfoils at Low Reynolds Numbers," 55th AIAA Aerospace Sciences Meeting, 2017, p. 0716.
- [2] Taha, H. E., and Rezaei, A. S., "Unsteady Viscous Lift Frequency Response Using The Triple Deck Theory," 2018 AIAA Aerospace Sciences Meeting, 2018, p. 0038.
- [3] Ramezanian, D., Reza Ahrabi, B., and Mavriplis, D., "An Order N log N Parallel Newton–Krylov Solver for Time Spectral Problems," 23rd AIAA Computational Fluid Dynamics Conference, 2017, p. 4509.
- [4] Hussein, A. A., Taha, H. E., Ragab, S., and Hajj, M. R., "A variational approach for the dynamics of unsteady point vortices," *Aerospace Science and Technology*, Vol. 78, 2018, pp. 559–568.
- [5] Hammer, P., Altman, A., and Eastep, F., "Validation of a Discrete Vortex Method for Low Reynolds Number Unsteady Flows," *AIAA Journal*, Vol. 52, No. 3, 2014, pp. 643–649.
- [6] Ramesh, K., Gopalarathnam, A., Granlund, K., Ol, M. V., and Edwards, J. R., "Discrete-vortex method with novel shedding criterion for unsteady aerofoil flows with intermittent leading-edge vortex shedding," *Journal of Fluid Mechanics*, Vol. 751, 2014, pp. 500–538.
- [7] Moored, K. W., "Unsteady Three-Dimensional Boundary Element Method for Self-Propelled Bio-Inspired Locomotion," *Computers & Fluids*, Vol. 167, 2018, pp. 324–340.
- [8] Shehata, H., Zakaria, M., Hussein, A., and Hajj, M. R., "Aerodynamic Analysis of Flapped Airfoil at High Angles of Attack," 2018 AIAA Aerospace Sciences Meeting, 2018, p. 0037.
- [9] Kamemoto, K., "On Contribution of Advanced Vortex Element Methods Toward Virtual Reality of Unsteady Vortical Flows in the New Generation of CFD," *Journal of the Brazilian Society of Mechanical Sciences and Engineering*, Vol. 26, No. 4, 2004, pp. 368–378.
- [10] Dung, D. V., Zuhal, L. R., and Muhammad, H., "Two-Dimensional Fast Lagrangian Vortex Method for Simulating Flows around a Moving Boundary," *Journal of Mechanical Engineering*, Vol. 12, No. 1, 2015, pp. 31–46.
- [11] Wu, J. C., "Theory for Aerodynamic Force and Moment in Viscous Flows," AIAA Journal, Vol. 19, No. 4, 1981, pp. 432-441.
- [12] Rezaei, A. S., and Taha, H. E., "Transition regime and its effects on the unsteady aerodynamic characteristics of a pitching airfoil," 2019 AIAA Science and Technology Forum and Exposition, 2019. Manuscript submitted for publication.
- [13] Katz, J., and Plotkin, A., Low-Speed Aerodynamics, Cambridge University Press, 2001.
- [14] Shen, S. F., and Crimi, P., "The theory for an oscillating thin airfoil as derived from the Oseen equations," *Journal of Fluid Mechanics*, Vol. 23, No. 3, 1965, pp. 585–609.
- [15] Yates, J. E., "Viscous Thin Airfoil Theory and the Kutta Condition," AIAA 16th Aerospace Sciences Meeting, 1978, p. 152.
- [16] Yates, J. E., "Unsteady Viscous Thin Airfoil Theory," Tech. rep., Advisory Group for Aerospace Research and Development, 1978.